Catalysis Today 337 (2019) 3–14

Contents lists available at ScienceDirect

Catalysis Today

journal homepage: www.elsevier.com/locate/cattod

Burning questions of plasma catalysis: Answers by modeling

Annemie Bogaerts[a,*], Quan-Zhi Zhang[a], Yu-Ru Zhang[a,b], Koen Van Laer[a], Weizong Wang[a,c]

[a] Research Group PLASMANT, Department of Chemistry, University of Antwerp, Universiteitsplein 1, BE-2610, Wilrijk-Antwerp, Belgium
[b] Key Laboratory of Materials Modification by Laser, Ion, and Electron Beams (Ministry of Education), School of Physics, Dalian University of Technology, Dalian, 116024, People's Republic of China
[c] School of Astronautics, Beihang University, 100191, Beijing, People's Republic of China

ARTICLE INFO

Keywords:
Plasma catalysis
Packed bed reactor
Catalyst pores
Fluid modeling
Particle-in-cell/Monte Carlo collision simulations
Plasma streamer

ABSTRACT

Plasma catalysis is promising for various environmental, energy and chemical synthesis applications, but the underlying mechanisms are far from understood. Modeling can help to obtain a better insight in these mechanisms. Some burning questions relate to the plasma behavior inside packed bed reactors and whether plasma can penetrate into catalyst pores. In this paper, we try to provide answers to these questions, by means of both fluid modeling and particle-in-cell/Monte Carlo collision simulations. We present a short overview of recent findings obtained in our group by means of modeling, i.e., the enhanced electric field near the contact points and the streamer propagation through the packing in packed bed reactors, as well as the plasma behavior in catalyst pores, to determine the minimum pore size in which plasma streamers can penetrate.

1. Introduction

In recent years, plasma catalysis is gaining increasing interest for various environmental, energy and chemical synthesis applications, such as air pollution control, volatile organic compound (VOC) remediation, CO_2 and/or CH_4 conversion into value-added chemicals, and NH_3 synthesis [1]. However, there are still many unresolved questions about the underlying mechanisms of plasma catalysis [2,3]. It is known that the catalyst, and catalytic packing materials, affect the plasma behavior, and vice versa, the plasma also affects the catalyst. More specifically, the effects of plasma on the catalyst include:

(i) changes in the physicochemical properties of the catalyst, such as a higher adsorption probability [4], a higher surface area [5], a change in the oxidation state [6], reduced coke formation [7], and a change in the work function due to the presence of a voltage and current (or charge accumulation) at the catalyst surface [8];
(ii) the formation of hot spots, modifying the local plasma chemistry [9];
(iii) lower activation barriers, due to the existence of short-lived active species, such as radicals and vibrationally excited species [6].

Vice versa, the catalyst and catalytic packing may affect the plasma behavior in the following ways:

(i) enhancement of the local electric field in the plasma, because the catalyst is mostly present in a structured packing (e.g., pellets, beads, honeycomb,…; so-called packed bed reactor, typically in a dielectric barrier discharge, DBD), or simply due to the porosity of the catalyst surface [9–11];
(ii) change of the discharge type from streamers inside the plasma to streamers along the catalyst surface, resulting in more intense plasma around the contact points [12–15];
(iii) formation of microdischarges in the catalyst pores, resulting in more discharge per volume, increasing the mean energy density of the plasma [9,16];
(iv) adsorption of plasma species on the catalyst surface, affecting the residence time and hence the concentration of species in the plasma [17], while new reactive species might be formed at the catalyst surface.

In this paper, we will focus on how the catalyst and packing materials affect the plasma behavior, more specifically, resulting in electric field enhancement and a change in discharge type in a packed bed DBD reactor. Furthermore, we will also try to provide an answer to the burning question of whether plasma (streamers) can penetrate into catalyst pores and what is the minimum pore size needed for this. For this purpose, we will present recent results obtained in our group, from both fluid modeling and particle-in-cell / Monte Carlo collision (PIC/MCC) simulations, all carried out at atmospheric pressure.

* Corresponding author.
E-mail address: annemie.bogaerts@uantwerpen.be (A. Bogaerts).

https://doi.org/10.1016/j.cattod.2019.04.077
Received 28 December 2018; Received in revised form 31 March 2019; Accepted 23 April 2019
Available online 24 April 2019
0920-5861/

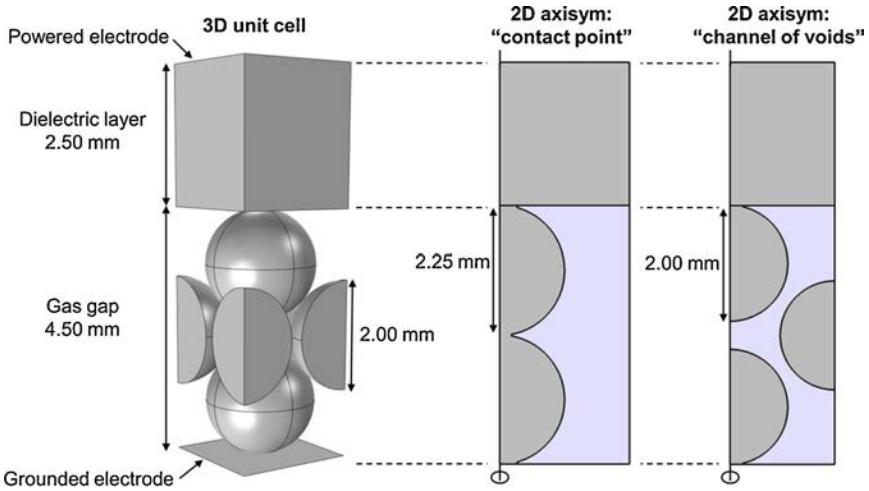

Fig. 1. 3D unit cell of a packed bed DBD reactor (left) and its 2D representations used in the "contact point" model (middle) and "channel of voids" model (right), used for the fluid simulations of the packed bed DBD reactor. Reproduced with permission from [29].

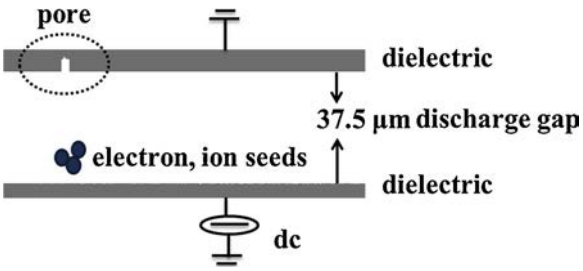

Fig. 2. Schematic illustration of the simulation geometry for modeling the behavior of plasma streamers in catalyst pores in a DBD reactor, by 2D PIC/MCC simulations.

In literature, the plasma behavior in a packed bed DBD reactor has been studied by a number of groups, both experimentally, e.g., by Kim et al. [12,18–20] and Tu et al. [21] using an intensified charge coupled device (ICCD) camera, as well as computationally [22–35]. Because the packing material (e.g., beads or pellets) is typically dielectric, the applied electric field between both electrodes of the DBD reactor causes polarization of the dielectric beads. Hence, opposite charges are present at the contact points between the beads, which might cause a strong local electric field enhancement in the plasma.

As experimental measurements in a packed bed DBD reactor are not straightforward, e.g., due to visual blocking of optical diagnostics by the packing beads, computer modeling can give useful additional insights. Chang [22] used a zero-dimensional (0D) plasma chemistry model for a $N_2/NF_3/O_2/H_2$ mixture in a $BaTiO_3$ packed bed plasma reactor, simply assuming an enhancement factor of the electric field in the voids between the pellets, deduced from the ratio of the dielectric constant of the pellets and the gas phase. Takaki et al. [23] presented a simplified time-averaged 1D model for N_2, based on solving the transport equations and Poisson's equation. Kang et al. [24] developed a 2D fluid model of a DBD reactor with two stacked ferroelectric beads, to study the propagation of microdischarges during the first 20 ns. Russ et al. [25] simulated transient microdischarges in a packed bed DBD reactor filled with dry exhaust gas, by means of a 2D fluid model, focusing again on a short time-scale (few tens of nanoseconds). Babaeva et al. showed very interesting modelling results for the effect of dielectric spheres blocking a plasma streamer, using a 2D fluid model in humid air [26]. Kruszelnicki et al. [27] applied 2D fluid simulations in humid air for a packed bed reactor with dielectric rods, studying the mechanism of discharge propagation. Finally, Kang et al. [28] also presented a 2D fluid model for studying surface streamer propagation in a simplified packed bed reactor, and compared the calculation results with time-resolved ICCD imaging data.

Within our group PLASMANT, we developed two complementary 2D fluid models, i.e., a so-called "contact point" model and a "channel of voids" model, to properly account for the characteristics of a 3D packed bed DBD reactor [29], and we studied the effect of dielectric

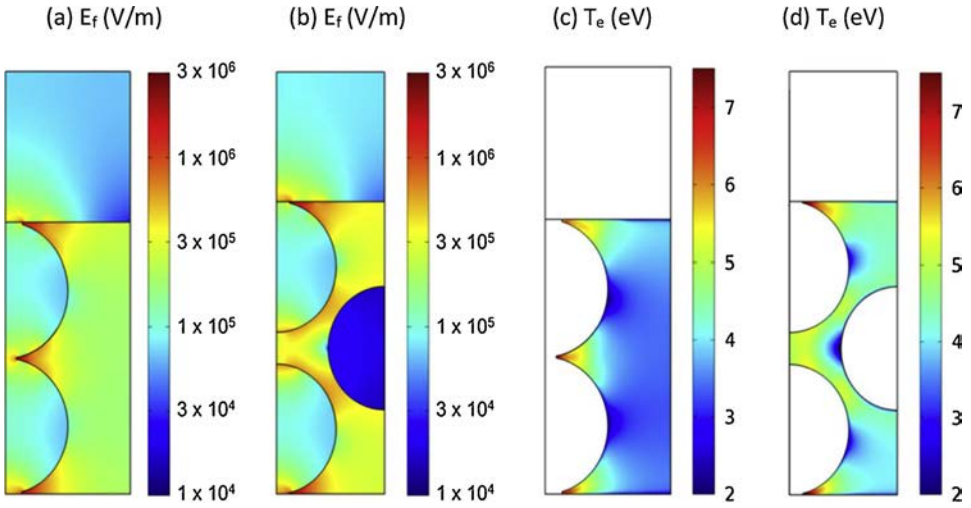

Fig. 3. Calculated time-averaged electric field (E_f; a, b) and electron temperature (T_e; c, d) in a packed bed DBD reactor in helium, obtained from two complementary 2D fluid models [29], to mimic best the real 3D geometry, i.e., with two beads in contact with each other (so-called "contact point" model) (a, c), and with three beads, not entirely in contact with each other, allowing a channel of voids where the gas can pass through (so-called "channel of voids" model) (b, d), at a peak-to-peak voltage of 4 kV and a frequency of 23.5 kHz.

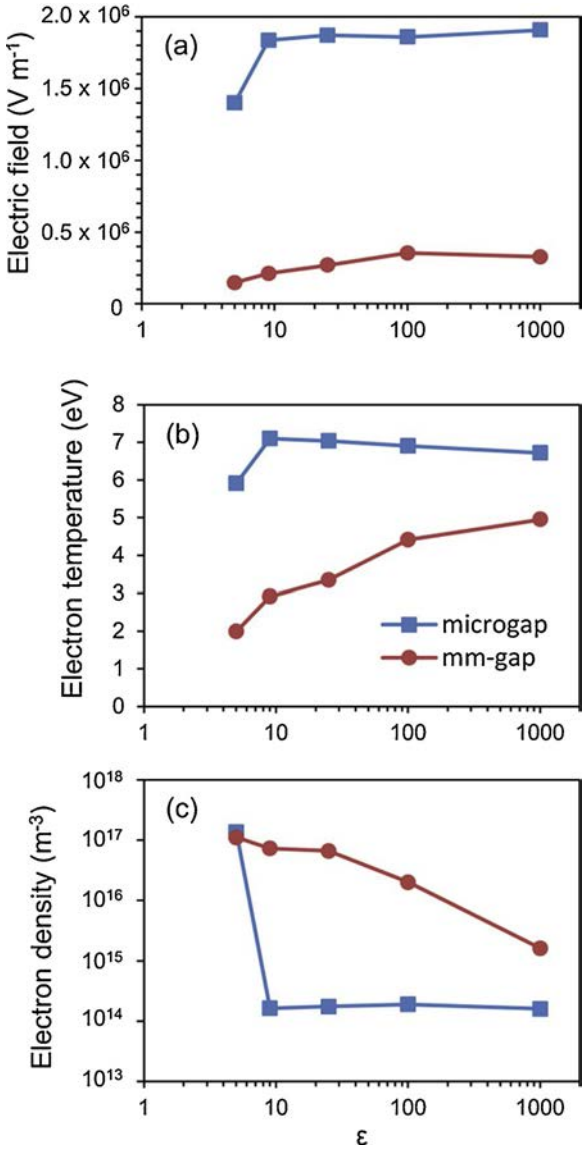

Fig. 4. Calculated space- and time-averaged electric field strength (a), electron temperature (b), and electron density (c), as a function of the dielectric constant of the packing beads (ε), obtained with a fluid model in helium, for both a microgap (500 μm) and a mm-gap (4.5 mm) packed bed DBD reactor, with the same applied voltage of 7.5 kV (peak-to-peak). Reproduced with permission from [30].

constant, bead size and gap size, on the electric field enhancement, electron temperature and electron density [30,31]. We also studied plasma streamer propagation in a packed bed DBD in air, for packing beads with different dielectric constants [32]. In addition, we applied 2D PIC/MCC simulations to describe the filamentary discharge behavior in a parallel-plate packed bed DBD reactor in air, and compared the simulation results with an unpacked DBD reactor [33]. The same model was also used to study the mode transition from volume to surface discharge upon changing applied voltage and O_2/N_2 mixing ratio [34]. Finally, besides packing beads, more sophisticated structures are also gaining interest for plasma catalysis, such as honeycomb packing and three-dimensional fiber deposition (3DFD) structures, so we also applied PIC/MCC simulations to study the streamer propagation in these structures [35]. We will show some of these simulation results in Sections 3.1 and 3.2 below.

Besides the plasma behavior in packed bed reactors (or in reactors with more sophisticated structures), another burning question is

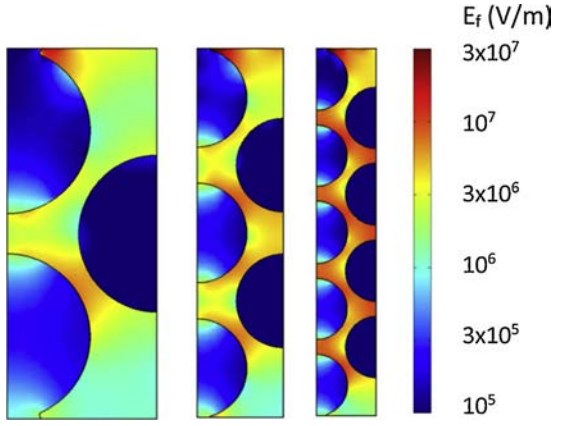

Fig. 5. Calculated time-averaged electric field strength for a packed bed DBD reactor in helium, with 3, 5 and 9 beads, with dielectric constant of 1000 (~ $BaTiO_3$ packing), as obtained with a fluid model [31]. The gap size is 4.5 mm, and the applied voltage is 7.5 kV (peak-to-peak).

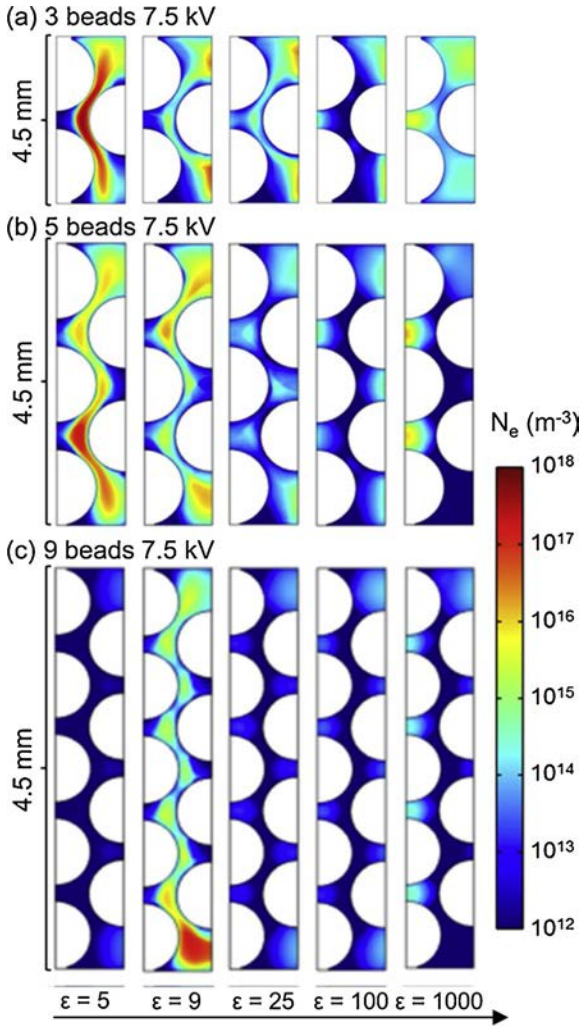

Fig. 6. Calculated time-averaged electron density profiles for a packed bed DBD reactor in helium, with 3, 5 and 9 beads, for different dielectric constants, as obtained with a fluid model [31]. Note that the different geometries have the same actual gap size (4.5 mm), but it was enlarged for the smaller bead sizes, to better visualize the behavior.

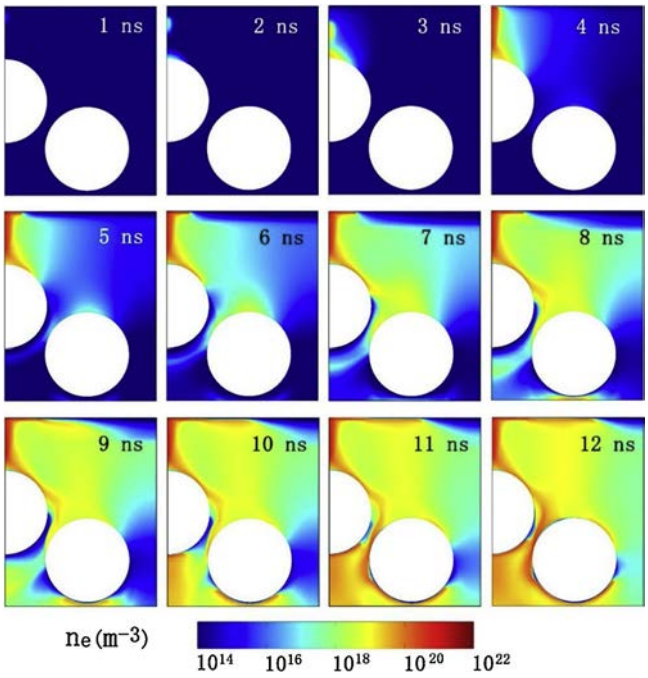

Fig. 7. Calculated electron number density evolution as a function of time, as obtained with a fluid model, for a packed bed DBD reactor in dry air, with two packing beads of $\varepsilon = 5$, and applied voltage of -10 kV at the top electrode. Adopted from [32] with permission.

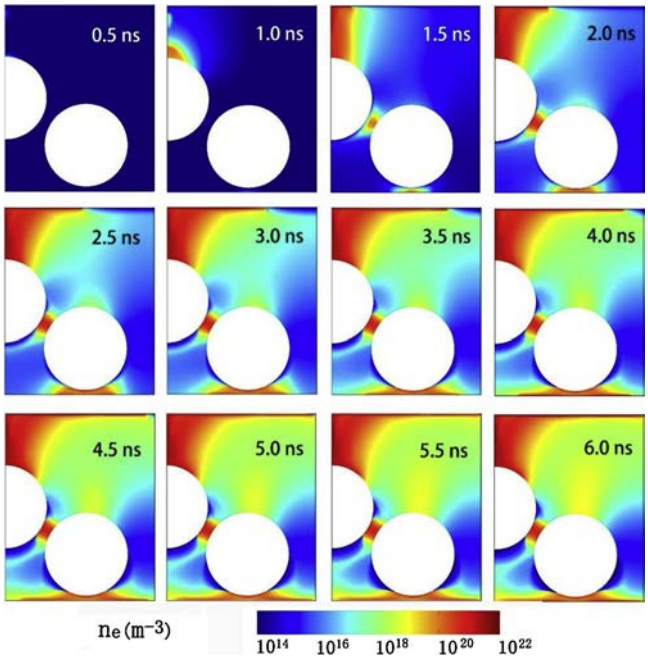

Fig. 8. Calculated electron number density evolution as a function of time, as obtained with a fluid model, for a packed bed DBD reactor in dry air, with two packing beads of $\varepsilon = 1000$, and applied voltage of -10 kV at the top electrode,. Adopted from [32] with permission.

whether plasma can penetrate into catalyst pores, because it defines the catalyst surface area exposed to the plasma (species), and thus the surface area available for plasma catalytic reactions. Several researchers have tried to answer this question by experiments. Holzer et al. reported that short-lived oxidants exist in the interior of porous catalysts, for typical pore sizes around 10 nm [36,37]. They concluded that these short-lived species might be formed inside the pores, if the electric field there was much stronger than in the bulk plasma. Alternatively, these short-lived species might be stabilized by adsorption on the pore inner surface during their diffusion inside the pores, significantly increasing their lifetime in the pores. The same authors also revealed the formation of strong microdischarges inside intra- and inter-particle pores (with particle size in the range of 1000–5000 μm) upon introducing ferroelectric pellets inside a plasma [9].

Hensel et al. [38] demonstrated that for a pore size of 0.8 μm, the discharge only developed on the dielectric surface (so-called surface discharge), while for a pore size of 15 μm, a transition in discharge mode was observed above the threshold voltage (i.e., 8.6 kV), and microdischarges inside the pores were observed. In addition, they studied the physical properties of microdischarges for various pore sizes, discharge powers, and gas mixtures, and they reported that the onset voltage of microdischarge formation decreases with increasing pore size [39]. In a follow-up study, they identified the pore size and the amplitude of the applied voltage as the critical parameters for microdischarge formation [16].

The above experimental studies are very important, but they cannot reveal the inherent mechanisms behind the formation of microdischarges in catalyst pores. For this purpose, modeling can again provide suitable answers.

Bhoj and Kushner developed a comprehensive multi-scale 2D fluid – surface kinetics model to describe the functionalization of rough polymer surfaces by an atmospheric pressure dielectric barrier – corona discharge in various gas mixtures [40–42]. Although it was not a catalyst, the surface roughness showed some similarities with catalyst pores. Furthermore, Wang et al. studied the propagation of an air plasma through a porous dielectric sheet, with a pore diameter of 100 μm, by means of a fluid model [43]. Finally, Cheng et al. applied fluid modeling to study the intersection of a negative streamer produced by an air DBD with bacteria biofilm on an apple surface, which is also characterized by a porous structure with dimensions in the order of 100 μm [44]. The authors found that ionization near the biofilm facilitates propagation of the streamer when the streamer head is 1 mm from the biofilm. The plasma could penetrate into the cavity of the biofilm, resulting in a uniform distribution of reactive oxygen and nitrogen species inside the cavity.

Within our group PLASMANT, we also developed a 2D fluid model for the plasma behavior inside catalyst pores with μm dimensions, in a helium DBD [45], and we studied the effect of different dielectric constants of the support material [46] and of the pore shape [47]. In addition, we performed PIC/MCC simulations to investigate plasma streamer penetration inside catalyst pores of both μm and nm sizes [48–50], for a DBD operating in dry air in filamentary mode. We will show results of both models in Section 3.3 below.

2. Computational details

2.1. Fluid modeling

To describe the plasma behavior in a packed bed DBD reactor, we first developed a fluid model in helium [29], (i) because of the simplified plasma chemistry, thus reducing the calculation time, and (ii) because helium yields a homogeneous discharge in a DBD, which is easier to describe with a fluid model. Later, we also developed a fluid model in air, to study in more detail the behavior of streamer propagation in the packed bed DBD reactor [32].

These fluid models solve conservation equations for the densities of the various plasma species. In the helium model, we considered six different species (i.e., He atoms, He^+ and He_2^+ ions, metastable He* atoms, He_2* dimers and the electrons), while in the air plasma, we took into account 15 different species (i.e., N_2, O_2, N, O, N_2^+, O_2^+, O^+, four N_2 electronically excited states (N_2 ($A^3\Sigma$), N_2 ($B^3\Pi$), N_2 ($C^3\Pi$) and N_2 ($a'^1\Sigma$)), one excited state of atomic O (O^1D), as well as NO, O_3 and the electrons).

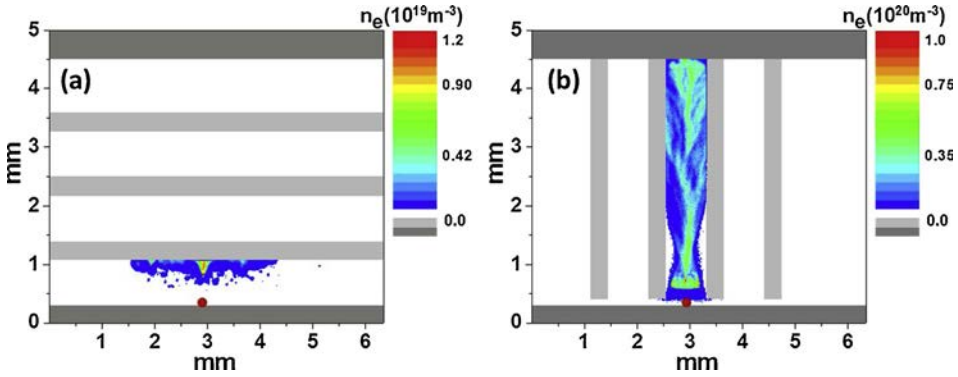

Fig. 9. Calculated electron number density profile (m^{-3}), illustrating the formation of a plasma streamer in a DBD reactor in dry air, with honeycomb monolith structure with channels parallel (a) and perpendicular (b) to the electrodes, as obtained from PIC/MCC simulations [35]. The red spot indicates the location of the seed particles (i.e., where the streamer is initiated). The dielectric plates covering the electrodes are depicted in dark grey colour, while the honeycomb structure is in light grey colour (For interpretation of the references to colour in this figure legend, the reader is referred to the web version of this article).

We also solve a conservation equation for the average electron energy, while the other plasma species, i.e., the so-called heavy particles, are assumed to be in thermal equilibrium with the gas, so that no extra energy conservation equation is needed for them. The conservation equations for the species densities are based on source and loss terms, defined by the chemical reactions, while the source of the electron energy is due to heating by the electric field, and the energy loss is again dictated by collisions. In addition, transport of the species is described by diffusion and by migration in the electric field (for the charged species). These conservation equations are coupled with Poisson's equation for a self-consistent calculation of the electric field distribution from the charged species densities. The packing beads are treated as solid objects in the model, with zero space charge and certain dielectric properties inside the beads, as well as charge accumulation on their surface. These models were developed with the COMSOL Multiphysics Simulation Software. More details can be found in [29,32].

In principle, a packed bed DBD reactor needs to be modeled in three dimensions (3D), to fully account for the packing geometry, as there is no axial symmetry to reduce the geometry to 2D. However, the mesh size for modeling a packed bed DBD reactor needs to be very small, to account for the regions near the contact points between the beads, yielding up to 100,000 mesh elements even in a 2D geometry [29]. Hence, modeling a packed bed DBD reactor in 3D is not yet feasible within a realistic calculation time. Therefore, we developed two complementary axisymmetric 2D fluid models, in order to approach the 3D geometry, i.e., a so-called "contact point" model and a "channel of voids" model; see Fig. 1 [29]. The combination of these two models allows us to describe the two important features of a packed bed DBD reactor, i.e., (i) the contact between the beads, which is expected to enhance the local electric field in the discharge due to polarization effects, and (ii) the fact that the voids between the beads are connected, allowing the plasma to travel from one side of the discharge gap to the other.

To describe the plasma behavior inside catalyst pores, we applied a similar fluid model in helium, with the same equations as explained above. For a self-consistent description, we should not only focus on the pore region, but we must take into account the entire discharge gap. This causes some challenges in terms of mesh size. Indeed, we assumed a DBD reactor with gap of 2 mm, while the pores have μm-dimensions. Therefore, we had to use different mesh sizes: we used a non-uniform mesh distribution (so-called structured mesh) in the bulk region (with mesh size of 15 μm), which was refined to 2 μm near the top and bottom dielectric plates. In addition, we used a mesh of about 0.5 μm near and inside the pores, which are assumed to have dimensions of 10 μm and larger. This mesh distribution allowed to simultaneously resolve both reactor-scale and surface-scale processes. More details about this model can be found in [45].

2.2. Particle-in-cell/Monte Carlo collision (PIC-MCC) simulations

PIC/MCC simulations describe the behavior of electrons and ions (i.e., their trajectory and collisions) during successive time-steps. From their positions in the discharge region, we obtain the space charge density, which is used to calculate the electric field distribution from Poisson's equation. This electric field is used to calculate the trajectory of the ions and electrons during the next time-step, and so on. It is not possible to follow all the individual electrons and ions in PIC/MCC simulations, because of excessive calculation times. Therefore, we follow a number of super-electrons and super-ions, which represent the real number of electrons and ions, defined by their weight. We apply here a 2D implicit PIC/MCC model, and a detailed description about this model can be found in [51,52].

For modeling plasma streamer propagation inside catalyst pores, we used square cells in the model. The geometry is schematically illustrated in Fig. 2. It is 50 μm in height, and 37.5 or 90 μm in radius (depending on the pore size under study; see details in [49]). Indeed, like in the fluid model description above, we had to include the entire discharge gap between the electrodes, to be able to properly describe the streamer propagation in the discharge, before it can enter the pore. The electrodes are covered by dielectric plates. A negative DC voltage is applied to the bottom electrode, while the top electrode is grounded. As shown in Fig. 2, a small pore is present in the top dielectric. When simulating the plasma behavior with a 50 nm diameter pore, we uniformly divided the simulation region (of 50 μm × 37.5 μm) into 2049 × 1500 cells, with a mesh size around 25 nm. This number of cells is limited by the computation time and computer memory (see below).

We applied the model to dry air, with a constant density of background molecules (O_2, N_2) at 300 K. We trace free electrons, N_2^+, O_2^+, O_2- during the whole simulation. The streamer is initiated by artificially placing 20 seed electrons, 20 O_2^-, 20 O_2^+, and 20 N_2^+ ions right above the bottom dielectric (see Fig. 2), with initial velocities sampled from a Maxwellian distribution. Their initial weight is 1 (i.e., 1 super-particle corresponds to 1 electron or ion), but it automatically increases with the streamer evolution, by a particle merging algorithm: when the number of super-electrons or super-ions exceeds 40 in each grid, three particles are combined into two particles with both conservation of momentum and energy. Typically, the weights increase up to 10^6 for both electrons and ions, when the streamer has arrived at the top dielectric. When the electrons and ions arrive at the dielectric, they accumulate on the dielectric surface and contribute to surface charging, as explained in detail in [49].

The simulation time-step is fixed at 10^{-14} s, and the total simulation time ranges till ca. 20 ps, which is enough to allow the plasma streamer to arrive at the top dielectric and penetrate till the bottom of the catalyst pore, in our simulated geometry. Note that we simply assumed a pore in a dielectric material (with varying dielectric constants); hence not a real catalytic material, but rather a catalytic support material. Catalytic surface reactions are also not yet included in our model.

We take into account 23 different reactions of the electrons with N_2

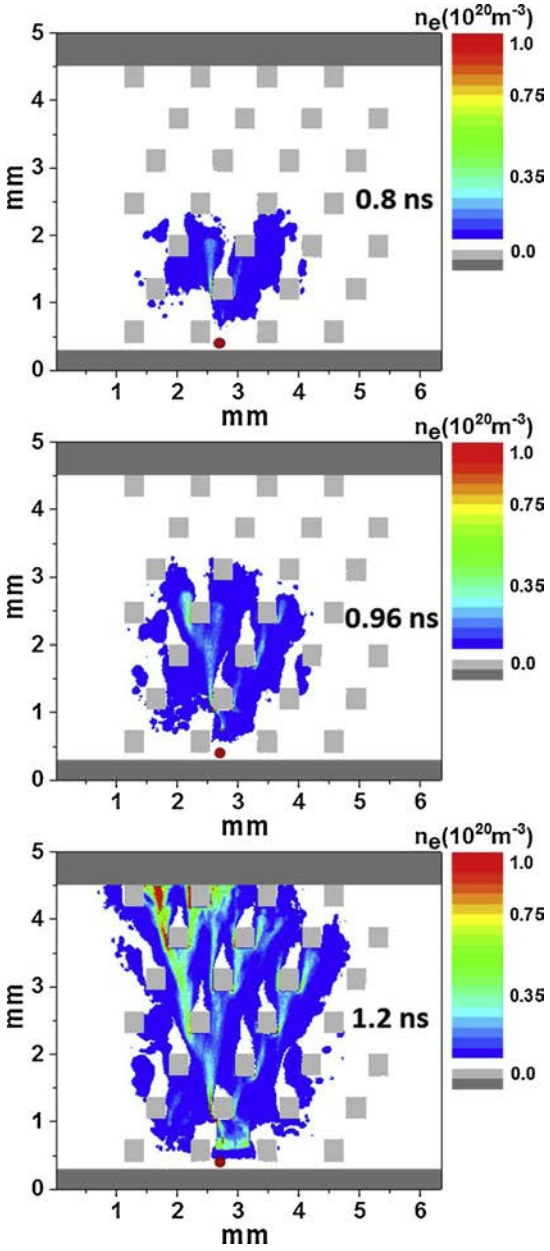

Fig. 10. Calculated electron number density profile (m^{-3}), at different times, illustrating the evolution of a plasma streamer in a DBD reactor in dry air, with 3DFD 1–3-5 stacking architecture, as obtained from PIC/MCC simulations [35]. The red spot indicates the location of the seed particles (i.e., where the streamer is initiated). The dielectric plates covering the electrodes are depicted in dark grey color, while the fibers of the 3DFD structure are in light grey color. It is clear that the streamers can distribute to different channels, yielding a broad plasma distribution (For interpretation of the references to colour in this figure legend, the reader is referred to the web version of this article).

and O_2, i.e., elastic collisions, 5 electron impact electronic excitation reactions with O_2 and 13 electron impact electronic excitation reactions with N_2, as well as electron impact ionization of N_2 and O_2, and electron attachment with O_2, see [48] for more details. Photoionization is taken into account by a widely used stochastic version of Zhelenyak's photoionization model [53,54], which describes ionization of O_2 molecules after absorbing photons with a wavelength between 98 and 102.5 nm, which are emitted by excited N_2 molecules. However, photoionization was found to be negligible in this small discharge gap: the photoionization rate was much lower than the electron impact ionization rate, and the results were nearly the same with and without photoionization.

For describing plasma streamer propagation in a packed bed DBD, we used the same PIC/MCC simulation method. Details are given in [48]. In addition, we also applied the same model for studying a DBD with other structured packings, such as honeycomb monoliths and 3DFD structures. As the channel sidewalls in a honeycomb monolith are all closed, we can define a 2D simulated honeycomb monolith discharge geometry, either with the channels set perpendicular or parallel to the electrodes. Modelling a 3DFD structure in a 2D PIC/MCC model is, however, more complicated. Indeed, the 3DFD structure is constructed by stacking fibres layer by layer, parallel to the electrodes. We modelled different stacking architectures, such as 1-1 stacking, with straight channels in both the vertical and horizontal direction, as well as 1–3 and 1–3–5 stacking, where the fibres are shifted to some extent at different layers. This yields a simulation architecture with many curved channels, which may induce significant differences in the streamer propagation, as illustrated in Section 3.2 below. The exact way how we modelled the various 3DFD structures in a 2D model is explained in detail in [35].

3. Results and discussion

3.1. Electric field enhancement in packed bed DBD reactors

Fig. 3 shows the calculated time-averaged electric field and electron temperature distributions, in a helium packed bed DBD, as obtained from our fluid model, for a peak-to-peak voltage of 4 kV and a frequency of 23.5 kHz, in the 2D geometries of both the "contact point" model (a, b) and the "channel of voids" model (c, d), as described in Section 2.1 above (cf. Fig. 1 above). The local electric field enhancement near the contact points due to polarization of the beads is obvious, both inside the material and in the gas gap. It is most clearly illustrated in the "contact point" model (Fig. 3(a)). This enhanced electric field gives rise to more pronounced electron heating near the contact points, causing a higher electron temperature, as seen in Fig. 3(c). The same behavior is also predicted by the "channel of voids" model (Fig. 3(b, d)), albeit somewhat less pronounced, because the beads are not in direct contact with each other.

At this relatively low applied voltage of 4 kV, the plasma is initiated at the contact points, and remains in this region, reflecting the properties of a Townsend discharge. Note that in this case, the electric fields obtained in the voids between the beads are lower than expected for a typical DBD plasma (hence reflecting the Townsend discharge). Indeed, an electric field of 3×10^5 V/m corresponds to a reduced electric field (E/N) of 12 Td (1 Td = 10^{-21} V m^2), at atmospheric pressure and room temperature, while a DBD is typically characterized by reduced electric fields above 100 Td (corresponding to electric field values around 3×10^6 V/m, as found near the contact points in this case).

At higher applied voltage, the electric fields will be higher, more typical for a DBD (see also below), and the discharge will spread out more into the bulk of the reactor, from one void space to the other, as was illustrated in [29]. This is in qualitative agreement with ICCD camera experiments from Kim et al. [18,19] and Tu et al. [21], which also reported that at low applied voltage the discharge stays local at the contact points, while at higher voltage, it spreads across the surface of the packing material.

We also varied the dielectric constant (ε) of the packing beads, to study its effect on the plasma characteristics, for two different gap sizes, i.e., a mm-gap (4.5 mm) and a microgap (500 μm) [30]. We only used the "channel of voids" model for this study, because it captures both characteristics of a packed bed DBD, being the enhanced electric field and electron temperature near the contact points, as well as the spreading of the discharge between the beads (see Fig. 3 above)."

Fig. 4 illustrates the calculated time- and space-averaged electric field, electron temperature and electron and ion densities as a function of ε, for both gap sizes. The calculations were performed for ε = 5, 9,

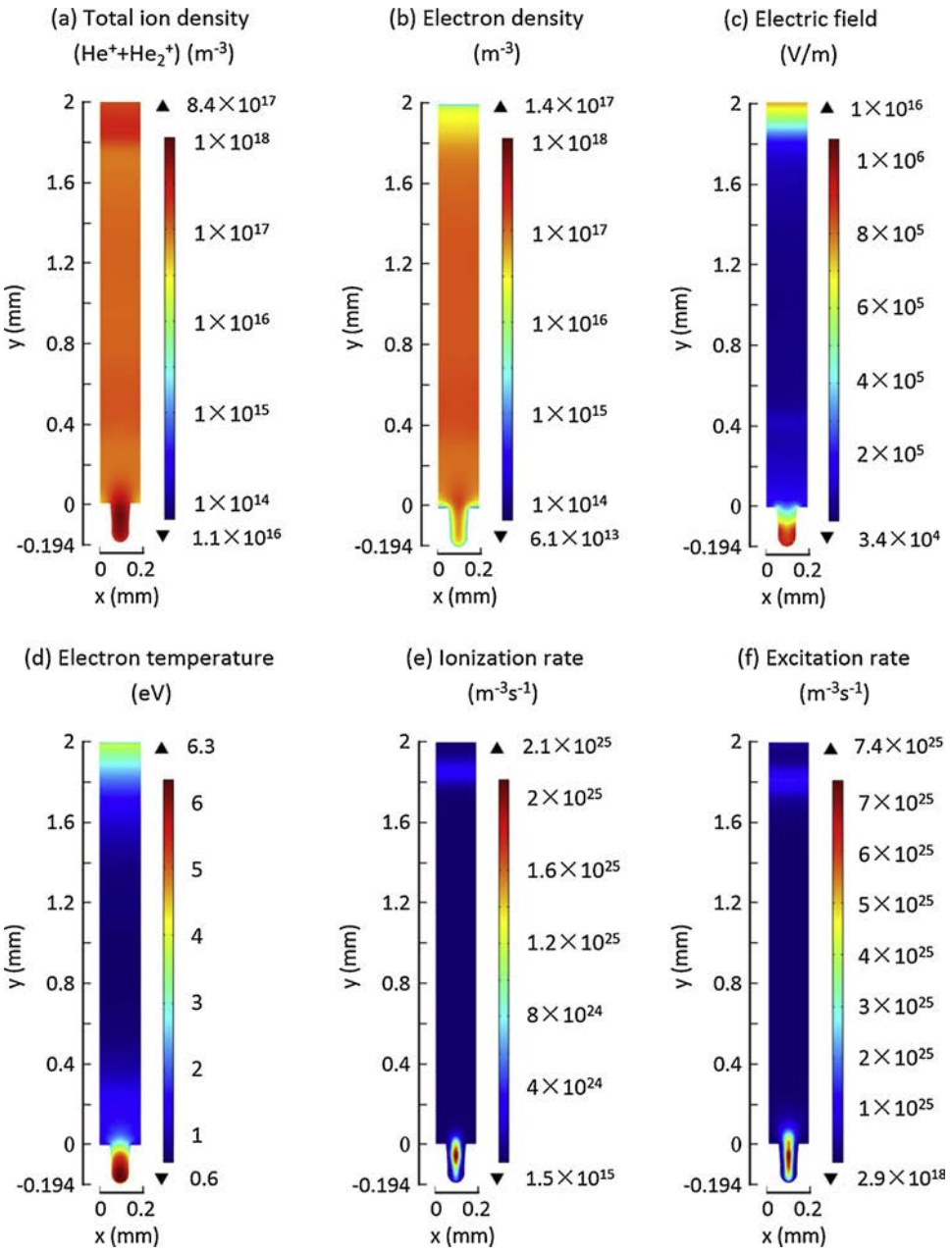

Fig. 11. Calculated distributions of the total ion density (a), electron density (b), electric field (c), electron temperature (d), electron impact ionization rate (e) and electron impact excitation rate, averaged over one period, as obtained from fluid modeling for a helium DBD with applied voltage of 20 kV, and with a 100 μm pore at the bottom dielectric (with dielectric constant of 9) [45]. Note that in (a) and (b) the same color scale is used, to allow comparison, but the values above and below the color scale indicate the maximum and minimum densities in each case, illustrating that the electron density is much lower inside the pore than the total ion density.

25, 100 and 1000, which are representative for silica (SiO_2), alumina (Al_2O_3), zirconia (ZrO_2), titania (TiO_2) and barium titanate ($BaTiO_3$) packing materials, respectively.

As appears from Fig. 4(a), the electric field is much more enhanced (at least a factor 5) in the microgap reactor, because the same voltage was applied in both cases, and hence it results in a stronger electric field for the shorter gap. This stronger electric field results in more current peaks per half cycle, as was illustrated in [30]. Indeed, the required electric field strength to cause a breakdown is more often reached in this case.

It is also clear from Fig. 4(a) that the calculated electric field increases upon higher dielectric constant of the packing beads in both gap sizes, but only up to a certain point. Indeed, our model predicts that for the higher dielectric constants, the electric field enhancement only occurs at the top part of the reactor, where the packing beads are in contact with the dielectric covering the powered electrode, while the electric field near the bottom (grounded) electrode is rather weak, due to less polarisation between the lower beads and the grounded electrode. This makes that the space- and time-averaged electric field does not continue to rise upon higher dielectric constant of the packing beads.

The calculated electron temperature (Fig. 4(b)) follows a similar trend as the electric field, which is logical, as the electrons are heated by the electric field. In the mm-gap reactor, the electron temperature rises gradually upon rising dielectric constant, but in the microgap reactor, the rise is only visible from $\varepsilon = 5$ to $\varepsilon = 9$, followed by a slight drop, attributed to the fact that the electric field enhancement mainly takes place at the top part of the reactor, as discussed above.

Finally, the calculated electron density (Fig. 4(c)) more or less follows the opposite trend as the electric field strength: it drops by three orders of magnitude between $\varepsilon = 5$ and 9 in the microgap reactor, while for the mm-gap reactor a more gradual drop is observed between $\varepsilon = 25$ and 1000. This drop is attributed to a change in discharge behavior. Indeed, upon rising dielectric constant, the plasma cannot travel anymore through the channels between the voids. In the mm-gap reactor, this change in discharge behavior occurs gradually for ε rising

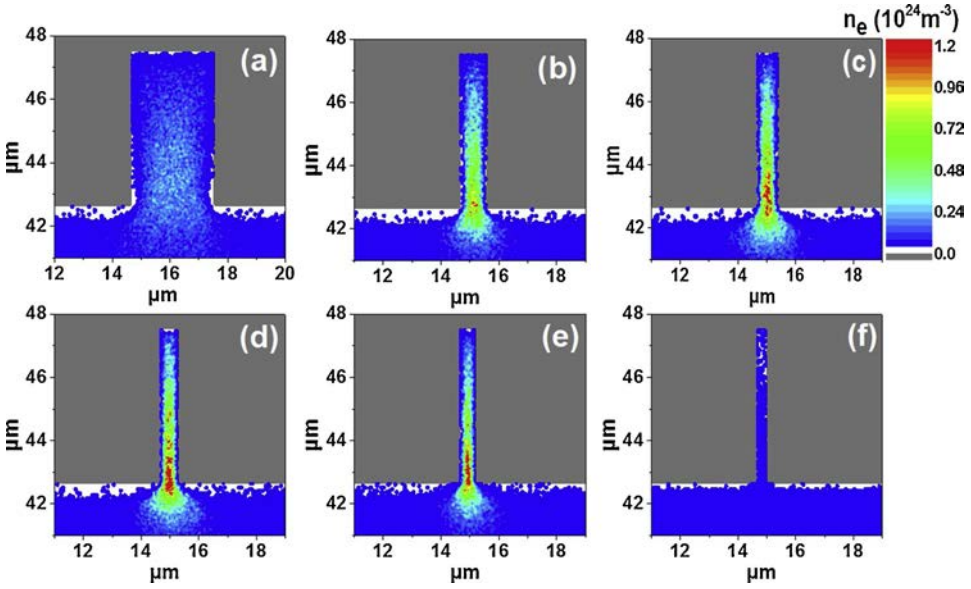

Fig. 12. Calculated electron density profiles, in (m^{-3}), near and inside a pore, with diameter of (a) 3 µm, (b) 1 µm, (c) 800 nm, (d) 700 nm, (e) 600 nm, (f) 400 nm, as obtained from PIC/MCC simulations in dry air, for an applied DC voltage of −8 kV [49].

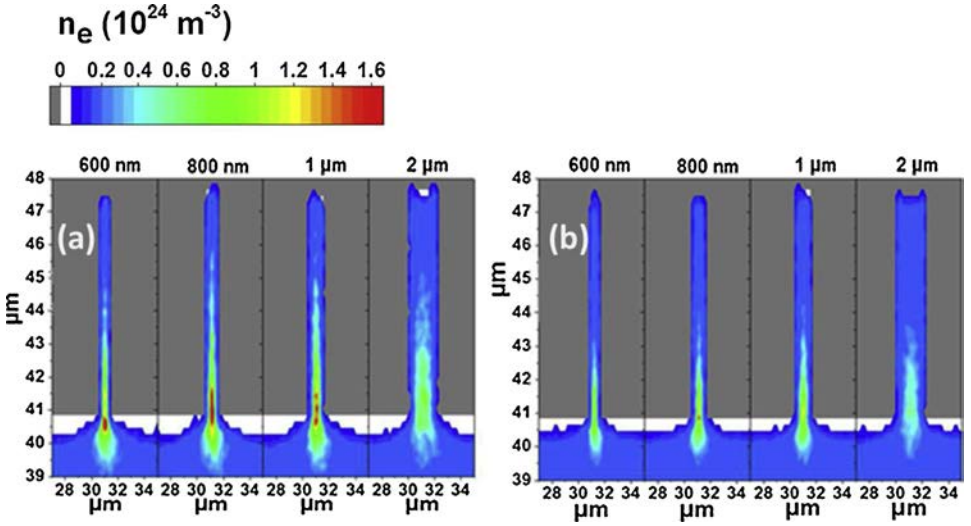

Fig. 13. Calculated electron density profile, in m^{-3}, near and inside a pore with diameter of 600 nm, 800 nm, 1 µm, and 2 µm, for $\varepsilon = 25$ (a), and $\varepsilon = 200$ (b), as obtained from PIC/MCC simulations in dry air, for an applied DC voltage of −8 kV [50].

from 25 to 1000, resulting in an overall lower electron density upon rising dielectric constant. In the microgap reactor, our model predicts that the plasma can only travel through the channels between the packing beads when $\varepsilon = 5$. This was illustrated in detail in [30]. Indeed, at higher dielectric constants, the electrons (and ions) get more easily absorbed at the walls and at the surface of the packing beads, due to the small dimensions and enhanced electric field. Hence, the plasma cannot travel anymore through the small channels between the packing beads, explaining the much lower averaged electron (and ion) density. The effect is more pronounced for the electrons, due to their smaller mass and thus higher mobility. This results in a non-quasineutral plasma.

We did not only vary the dielectric constant of the packing beads, but also the bead size, for a fixed interelectrode gap in a helium packed bed DBD. Fig. 5 illustrates that the electric field enhancement is more pronounced for smaller beads, which have more contact points. Note that the electric fields in the voids are now in the order of 2×10^6 V/m for the larger beads, rising to 10^7 V/m for the smaller beads, which corresponds to reduced electric field (E/N) values around 80–400 Td.

As illustrated in Fig. 4(a) above, the electric field enhancement in the mm-gap reactor is in general more pronounced for packing beads with larger dielectric constant. As a result, at low dielectric constant, the plasma is more spread out over the full discharge gap, with a significant density in the voids, as well as in the connecting void channels. Upon rising dielectric constant, the plasma becomes more localized in the voids, as is clear from Fig. 6. In addition, Fig. 6 clearly illustrates that for the larger beads, the shift from full gap discharge to localized discharges occurs at a higher dielectric constant than for the smaller beads. Finally, at $\varepsilon = 5$, the packed bed reactor with the smallest beads does not enable plasma formation at the applied voltage of 7.5 kV, as appears from Fig. 6(c). Indeed, a higher breakdown voltage is required to cause plasma formation, in case of small beads with low dielectric constant. Note that in general, the electron density is quite low, which is attributed to the large probability of electron losses at the surface of the beads, and the fact that these calculations were performed for helium, characterized by a uniform discharge. In air discharges, characterized by filaments, the electron density is typically higher inside the filaments, as illustrated below. More details about the plasma behavior in packed bed DBDs for different bead sizes and dielectric constants can

be found in [31].

Although these models are developed for helium, we expect a similar behavior in reactive gases, which are typically used in plasma catalysis applications. The electric field enhancement, and the resulting higher electron temperature, will affect the type of collisions in the plasma. Indeed, at higher electron temperature, more collision channels can come into play, when the electron energy is higher than the threshold energy for these collisions. For instance, electron impact ionization typically requires a higher threshold, and the maximum in the ionization cross section typically lies at higher electron energy, compared to electron impact excitation. Compared to a non-packed DBD, the same applied power thus yields a higher electron temperature, allowing a wider variety of electron impact collisions, which can activate the gas molecules (by excitation, ionization and dissociation). This might explain why a packed bed DBD reactor typically yields higher pollutant decomposition or CO_2 conversion than a non-packed reactor, at least at the same gas residence time [55,56]. When comparing at the same flow rate, however, the gas residence time in a packed bed reactor is considerably reduced compared to a non-packed reactor, and hence, the enhanced electric field might not always be sufficient to compensate for the shorter residence time, sometimes causing a drop in CO_2 conversion compared to a non-packed reactor [55,56].

3.2. Plasma streamer propagation in packed bed DBD reactors

To study the behavior of streamer propagation in a packed bed DBD reactor, we developed a 2D fluid model for a packed bed DBD in air [32]. Depending on the dielectric constant of the packing beads, our model either predicts more filamentary microdischarges or more surface discharges.

Indeed, at low dielectric constants (e.g., $\varepsilon = 5$), plasma ignition between the beads occurs as surface discharges or surface ionization waves, created due to electric field components parallel to the dielectric surfaces, resulting from surface charging. These surface ionization waves can connect with the surface of the adjacent beads, as illustrated in Fig. 7. On the other hand, at high dielectric constants (e.g., $\varepsilon = 1000$), our model predicts filamentary microdischarges that are constrained between the contact points of the beads, as shown in Fig. 8. Note that the electron density inside the microdischarge filaments is now much higher than obtained in Fig. 6 above, for a helium discharge, which does not exhibit a filamentary character. At intermediate dielectric constants, a mixed mode of surface discharges and local discharges was observed, as illustrated in [32]. The calculation results were in good qualitative agreement with experiments, as detailed in [32].

To summarize, the locally constrained filamentary microdischarges between the beads may limit the catalyst activation due to the limited catalyst surface area in contact with the plasma. Hence, it might have implications for the efficiency of plasma catalysis. Indeed, although the local electric field enhancement is typically most pronounced at high dielectric constants (see Fig. 4 above), the catalyst surface area in contact with the plasma is limited at these high dielectric constants, due to the localized discharges. Both effects will compete each other in terms of efficiency for the plasma and/or catalytic reactions, so depending on the relative importance of both effects, packing materials with a high or low or intermediate dielectric constant will perform the best, as indeed demonstrated in experiments (e.g., [55,56]).

Again, we only used the “channel of voids” model to study the streamer propagation, because it captures both characteristics of a packed bed DBD, being the enhanced electric field and electron temperature near the contact points, as well as the streamer propagation through the reactor. However, it means that there are no contact points between the beads in this model (as is indeed obvious from Figs. 7 and 8), while in reality, the streamers will “feel” the contact points between the beads as a physical barrier. Nevertheless, they will anyway find their way through the channels in between the beads, so the absence of contact points in the model will not affect the general trends predicted by the model, being the transition from surface discharges to local filamentary discharges upon rising dielectric constant.

Besides fluid modelling, we also applied PIC/MCC simulations to describe plasma streamer propagation through packed bed reactors in dry air, revealing similar trends [33,34]. In addition, we also studied plasma streamer propagation through DBD reactors with other structured packings, such as a honeycomb packing and three-dimensional fiber deposition (3DFD) structures, which might be very promising for plasma catalysis.

Fig. 9 illustrates the calculated plasma streamer propagation in a honeycomb monolith structure with the channels parallel (a) and perpendicular (b) to the electrodes, as obtained from PIC/MCC simulations. The red spot in the figure shows the location of the seed particles. In Fig. 9(a), the streamer first arrives at the dielectric of the monolith, and develops along the dielectric surface, yielding a surface discharge. The local maxima at the surface indicate discharge enhancements, caused by photoionization. However, as the plasma streamer can only develop within the short diameter (~0.8 mm) of one channel, the electron density is quite low, i.e. in the order of $10^{19}\,m^{-3}$.

In Fig. 9(b), the honeycomb channels are perpendicular to the electrodes. The calculated plasma streamer is obviously limited to one channel, indicating that the streamers in different channels of a honeycomb structured catalyst will be completely separated. However, compared to Fig. 9(a), the electron density is an order of magnitude higher, as the plasma streamer can develop over a much longer distance. This will yield a larger production of reactive plasma species upon electron impact reactions, and it may explain why in practice the channels are mostly perpendicular to the electrodes in plasma catalysis applications with honeycomb structured catalysts [16,57].

Finally, Fig. 10 shows the calculated plasma streamer propagation for a 3DFD structure with so-called 1–3–5 stacking architecture. In contrast to the separate channels of a honeycomb structured catalyst (Fig. 9), the streamers can now distribute to different channels, causing discharge enhancement due to surface charging on the dielectric walls of the structured catalyst, and especially giving rise to a broad plasma distribution, i.e., not limited to one channel as for the honeycomb structure. This broader plasma distribution should be beneficial for plasma catalysis, as it allows a larger catalyst surface area to be exposed to the plasma. More results about the streamer propagation in different 3DFD stacking architectures, including the effect of different positions of the seed particles (for streamer initiation), can be found in [35].

3.3. Plasma streamer penetration in catalyst pores

First we present some results of the fluid model in helium, for the plasma behavior in catalyst pores with μm sizes. Subsequently, we will show that plasma streamers can also penetrate in smaller pores, in filamentary discharges operating in air.

Fig. 11 illustrates the fluid calculation results. As explained in Section 2.1 above, the model is applied to the entire DBD gap of 2 mm, for self-consistent results. This puts constraints to the size of the pores that can be modeled. In addition, a fluid model cannot be applied to pores with nm dimensions, because the mesh size would be too small for a fluid description. Therefore, we focus here on a pore of 100 μm, but it should be noted that we applied the model to pores down to 10 μm diameter [45]. Smaller dimensions did not allow plasma formation inside the pores.

The total ion density (Fig. 11(a)) rises drastically inside the pore, reaching a maximum value 7 times higher than in the center of the discharge. The electron density exhibits a slight increase near the pore, but it drops to low values inside the pore (Fig. 11(b)), because the electrons are more easily lost at the walls due to their small mass, and also because the electric field pushes them back to the bulk region (see below).

The different electron and ion densities inside the pore result in a

significant space charge, which causes electric field enhancement inside the pore (Fig. 11(c)), yielding a pronounced rise in electron temperature as well (Fig. 11(d)). As a result, the electron impact ionization rate is also greatly enhanced inside the pore (Fig. 11(e)), which explains in turn the high ion density inside the pore. Note that the electrons are also formed inside the pore, but they are more easily lost at the walls, and pushed out of the pore due to the electric field, as mentioned above, explaining their much lower density. Finally, also the electron impact excitation rate in the pore is enhanced (Fig. 11(f)), yielding more excited species. Likewise, for a reactive gas, also the rate of electron impact dissociation will be enhanced, thus creating more radicals. Hence, our model predicts that for a pore size of 100 μm, the plasma species are effectively generated inside the pore. In addition, the ions will also migrate into the pore due to the strong electric field.

Our model predicts that plasma formation inside the pores occurs more easily at larger pore size and applied voltage [45], which was also observed by Hensel et al. [16,38]. A pore size of around 20 μm was predicted as the lower limit for plasma species formation inside the pore, at least for a helium plasma. The latter can be correlated with the Debye length, which is in the order of 40 μm for the typical conditions under study here (i.e., helium plasma with electron temperature and density of 3 eV and 10^{17} m^{-3}). In air filamentary discharges, characterized with higher electron density inside the streamers, and thus smaller Debye lengths, plasma streamers can penetrate into smaller pores, as will be shown below.

We also studied the plasma behavior for catalyst support materials with various dielectric constants [46]. We found that for a pore of 100 μm diameter, the ionization clearly takes place inside the pore for $\varepsilon \leq 200$, with a maximum reached at $\varepsilon = 50$. At $\varepsilon > 300$, the ionization does not occur inside the pore, but only in the sheath in front of the pore. The reason is that at these large dielectric constants, the polarization of the left sidewall counteracts that of the right sidewall, reducing the net electric field, and thus the electron temperature and electron impact ionization inside the pore. Furthermore, our model reveals that the ionization enhancement inside smaller pores than 100 μm only occurs for materials with smaller dielectric constants. For pore sizes of 50 μm, 30 μm and 10 μm, only materials with dielectric constants below 200, 150 and 50, respectively, seem to yield enhanced ionization inside the pores. Note that $\varepsilon = 300$ is a typical value for $SrTiO_3$, $\varepsilon = 200$ corresponds to $CaTiO_3$, and $\varepsilon = 50$ is a typical value for TiO_2 [58].

To our knowledge, no experiments are available for the plasma behavior inside catalyst pores with different dielectric constants. Hence, our model predictions still have to be validated by experiments, but they suggest that the most common catalyst supports, i.e., Al_2O_3 and SiO_2, with dielectric constants around 8–11 and 4, respectively, can more easily promote plasma formation inside catalyst pores than e.g., ferroelectric materials with dielectric constants above 300.

Finally, we also applied this model to study the plasma behavior inside catalyst pores with different pore shapes, and we found that the electric field is significantly enhanced near tip-like structures [47]. In general, the pore shape seems to greatly affect the electric field enhancement, and thus the plasma properties. More details about these simulations can be found in [47].

To summarize, our fluid model reveals that plasma species can only be created inside catalyst pores with dimensions above 10 μm, for materials with dielectric constants below 50. These pore sizes are of interest for structured catalysts, but catalytic supports typically have pores in the nm range, and the latter might thus be too small for plasma formation inside pores, according to our fluid model predictions. However, the above studies were applied to a helium plasma, which yields a homogeneous discharge. For plasma catalysis applications, reactive gases are more relevant, and they exhibit streamer formation, which are characterized by much higher electron densities, and thus smaller Debye lengths. Hence, it is well possible that in this case, plasma streamers can penetrate in nm-sized catalyst pores. This is too small to be treated by fluid simulations, so we developed a PIC/MCC model for an air plasma, accounting for streamer formation.

Fig. 12 shows the calculated electron number density profile inside pores with different diameters, as obtained from our PIC/MCC simulations, for an applied voltage of −8 kV. The electron density reaches a maximum inside the pores for pore diameters of 600 nm and above, while the electron density is negligible for the pore diameter of 400 nm. This indicates that, at the conditions under study here, plasma streamer formation occurs in pores with diameter of 600 nm and above, but not for smaller pores. This behavior can be explained by the Debye length.

Indeed, our PIC/MCC model reveals that the Debye length is an important criterion for plasma streamer penetration into catalyst pores, i.e., plasma streamers can only penetrate into pores with diameter larger than the Debye length. At the conditions shown in Fig. 12, the Debye length was calculated to be 415 nm, which explains why plasma streamers cannot penetrate into pores of 400 nm diameter, while they can penetrate into larger pores. In general, the Debye length depends on the electron density and temperature in the plasma streamer, but is in the order of a few 100 nm up to 1 μm at typical DBD conditions in air. Hence, this is the typical range of pore sizes in which plasma streamers can still penetrate, as indeed illustrated in Fig. 12. Note that for higher applied voltages, plasma streamers will be able to penetrate into smaller pores, due to the higher plasma density and thus shorter Debye length. This has consequences for plasma catalysis, as it determines the catalyst surface area exposed to plasma, and thus the plasma catalytic performance.

For pores in the range of ˜50 nm, our simulations predict that plasma can only penetrate to some extent and only at early stages, before the actual plasma streamer reaches the catalyst surface and a sheath is formed [49].

Our model reveals that surface charging (both of the dielectric surface and the catalyst pore sidewalls) plays a crucial role in the plasma distribution along the dielectric surface, as well as in streamer penetration and discharge enhancement inside catalyst pores. The importance depends on the dielectric constant of the material. This is illustrated in Fig. 13. At low dielectric constant (e.g., $\varepsilon = 25$; Fig. 13(a)), surface charging causes the plasma to spread along the dielectric surface and inside the pores, leading to somewhat deeper plasma streamer penetration, while for larger dielectric constants (or for metallic coatings), the discharge appears to be more localized, due to very weak surface charging (see e.g., for $\varepsilon = 200$ in Fig. 13(b)). More details on the effect of surface charging on plasma streamer penetration in catalyst pores can be found in [50].

4. Conclusion

In this paper, we gave a brief overview of recent results obtained in our group, from fluid modeling and PIC/MCC simulations, to provide answers to some burning questions in plasma catalysis, i.e., on how plasma behaves inside packed bed DBD reactors, and whether plasma can penetrate into catalyst pores, and what is the determining factor for this.

We showed that the electric field is enhanced near the contact points of the beads in a packed bed DBD reactor, due to polarization of the beads. The effect is more pronounced at higher dielectric constants, and for smaller discharge gaps, albeit only to a certain point, after which the electric field and electron temperature stay constant (or drop) upon rising dielectric constant. In addition, higher dielectric constants cause a more pronounced drop in overall electron density, and the plasma streamers behave as local filamentary discharges between the beads, while they behave as surface discharges around the packing beads at low dielectric constants. This will have consequences for plasma catalysis. Indeed, although the local electric field is typically more enhanced at high dielectric constants, the catalyst surface area exposed to the plasma is more limited, due to the localized discharges. Depending on the relative importance of these competing effects in

terms of efficiency for the plasma and/or catalytic reactions, packing materials with a high or low (or intermediate) dielectric constant will perform the best, as indeed demonstrated in experiments (e.g., [55,56]).

We also showed calculation results for plasma streamer propagation in more sophisticated packing geometries, like honeycomb and 3DFD structures. Our model predicts that plasma streamers are limited to one channel in a honeycomb packing, while in 3DFD structures, they can distribute to different channels, yielding a broad plasma distribution. This should be beneficial for plasma catalysis, as it allows a larger catalyst surface area to be exposed to the plasma.

To answer the burning question whether plasma can be formed in catalyst pores, our calculations reveal that plasma streamers can penetrate into catalyst pores when the pore diameter is larger than the Debye length. Filamentary discharges (e.g. in air) can have a very high electron density in the streamers (in comparison to homogeneous discharges, e.g. in helium), yielding a small Debye length, i.e., in the order of a 400 nm–1 μm, depending on local electron temperature and density. This means that plasma streamers can penetrate into catalyst pores of several 100 nm diameter. Smaller pores (with nm dimensions) might, however, still be reached by plasma species created above the pores, due to diffusion. Finally, our models reveal that materials with low dielectric constant allow plasma to penetrate into smaller pores than materials with higher dielectric constants. This also has consequences for plasma catalysis, as it determines the catalyst surface area exposed to plasma, and thus the plasma catalytic performance.

These examples illustrate how plasma modeling can be useful for a better understanding of the underlying mechanisms of plasma catalysis. It should be noted that we only focused in this paper on dielectric support materials. In the future, we want to incorporate metallic catalyst activation on the support materials. Indeed, our models predict that surface charging is a determining factor for streamer propagation and plasma enhancement, so the metallic catalyst activation will also affect the plasma behavior. Incorporating these metallic catalysts is, however, quite challenging, as they typically have nm-dimensions, making it quite demanding for the mesh size (in combination with the reactor dimensions) and thus for the calculation time.

In addition, we would also like to include catalytic surface reactions in our plasma models (see e.g., [59,60]). Incorporating a detailed chemistry in 2D fluid models is quite challenging in terms of calculation time, and this is even more the case for PIC/MCC simulations. Hence, we will first have to define the most important reactions. 0D plasma chemistry modeling can be very useful for this purpose. It can describe a detailed plasma and surface chemistry without too much computational cost, based on which reduced sets can be defined, as input for 2D fluid or PIC/MCC models. Although 0D models in principle do not take into account spatial variations, they can incorporate surface chemistry for plasma catalysis, as illustrated e.g., in [59,60]. The surface reaction rate coefficients can be obtained from atomic scale classical molecular dynamics simulations or density functional theory. This yields an approach very similar to so-called microkinetics modeling, which is quite common in thermal catalysis.

Our final aim is to incorporate such surface reactions in our 2D fluid and PIC/MCC models as well. Due to the extensive computation time of PIC/MCC models, we believe it will be very challenging to include a detailed surface chemistry for plasma catalysis modeling at the reactor scale (e.g., streamer propagation through packed bed DBD reactors), so we believe fluid models might be more appropriate for this purpose. However, when studying plasma streamer penetration into catalyst pores, we believe that PIC/MCC models are more appropriate, due to the small pore dimensions, easily reaching the limits of fluid modeling. Moreover, due to the small dimensions of such catalyst pores (e.g., up to 1 μm to be practically relevant), PIC/MCC simulations with surface chemistry should be feasible. Furthermore, to study the diffusion of plasma species into even smaller catalyst pores, MC simulations (without electric field) in the pore, coupled to detailed surface chemistry, could be applied.

In conclusion, we believe that various models should be combined: (i) 0D plasma chemistry models with incorporated catalytic surface chemistry, to gain detailed insight in the plasma + surface chemistry, and to produce reduced chemistry sets for higher-dimensional models, (ii) 2D (or even 3D, if the computation time would allow for it) fluid models for reactor scale modeling (e.g., plasma streamer propagation in packed bed DBD reactors), (iii) 2D or 3D PIC/MCC simulations for plasma streamer penetration into catalyst pores with dimensions of a few 100 nm (that allow plasma streamer penetration), (iv) 3D MC simulations for describing diffusion of plasma species in even smaller catalyst pores, and (v) atomic scale simulations for the chemical reactions of plasma species at a catalyst surface, providing surface reaction coefficients for the above models. Such a multi-level computational approach should allow us to obtain an overall picture of plasma catalysis.

Acknowledgments

We would like to thank H.-H. Kim for performing experiments to validate the modeling of streamer propagation in packed bed reactors. We acknowledge financial support from the TOP-BOF project of the University of Antwerp, the European Marie Skłodowska-Curie Individual Fellowships “GlidArc” and “CryoEtch” within Horizon2020 (Grant Nos. 657304 and 702604).

References

[1] E.C. Neyts, K. Ostrikov, M.K. Sunkara, A. Bogaerts, Plasma catalysis: synergistic effects at the nanoscale, Chem. Rev. 115 (2015) 13408–13446.
[2] J.C. Whitehead, Plasma-catalysis: the known knowns, the known unknowns and the unknown unknowns, J. Phys. D: Appl. Phys. 49 (2016) 243001.
[3] E.C. Neyts, A. Bogaerts, Understanding plasma catalysis through modelling and simulation—a review, J. Phys. D: Appl. Phys. 47 (2014) 224010.
[4] N. Blin-Simiand, P. Tardivaux, A. Risacher, F. Jorand, S. Pasquiers, Removal of 2-heptanone by dielectric barrier discharges—the effect of a catalyst support, Plasma Process. Polym. 2 (2005) 256–262.
[5] J.P. Hong, W. Chu, P.A. Chernavskii, A.Y. Khodakov, Cobalt species and cobalt-support interaction in glow discharge plasma-assisted Fischer-Tropsch catalysts, J. Catal. 273 (2010) 9–17.
[6] V. Demidyuk, J.C. Whitehead, Influence of temperature on gas-phase toluene decomposition in plasma-catalytic system, Plasma Chem. Plasma Process. 27 (2007) 85–94.
[7] S. Shang, G. Liu, X. Chai, X. Tao, X. Li, M. Bai, W. Chu, X. Dai, Y. Zhao, Y. Yin, Research on Ni/γ-Al_2O_3 catalyst for CO2 reforming of CH4 prepared by atmospheric pressure glow discharge plasma jet, Catal. Today 148 (2009) 268–274.
[8] C.-J. Liu, R. Mallison, L. Lobban, Nonoxidative methane conversion to acetylene over zeolite in a low temperature plasma, J. Catal. 179 (1998) 326–334.
[9] F. Holzer, K.D. Kopinke, U. Roland, Influence of ferroelectric materials and catalysts on the performance of non-thermal plasma (NTP) for the removal of air pollutants, Plasma Chem. Plasma Process. 25 (2005) 595–611.
[10] O. Guaitella, F. Thevenet, E. Puzenat, C. Guillard, A. Rousseau, C_2H_2 oxidation by plasma/TiO_2 combination: influence of the porosity, and photocatalytic mechanisms under plasma exposure, Appl. Catal. B: Environ. 80 (2008) 296–305.
[11] C.J. Liu, J.X. Wang, K.L. Yu, B. Eliasson, Q. Xia, B. Xue, Floating double probe characteristics of nonthermal plasmas in the presence of zeolite, J. Electrostat. 54 (2002) 149–158.
[12] H.H. Kim, J.-H. Kim, A. Ogata, Microscopic observation of discharge plasma on the surface of zeolites supported metal nanoparticles, J. Phys. D: Appl. Phys. 42 (2009) 135210.
[13] X. Tu, H.J. Gallon, M.V. Twigg, P.A. Gorry, J.C. Whitehead, Dry reforming of methane over a Ni/Al_2O_3 catalyst in a coaxial dielectric barrier discharge reactor, J. Phys. D: Appl. Phys. 44 (2011) 274007.
[14] T. Nozaki, N. Muto, S. Kado, K. Okazaki, Dissociation of vibrationally excited methane on Ni catalyst: part 2. Process diagnostics by emission spectroscopy, Catal. Today 89 (2004) 67–74.
[15] A. Mizuno, Generation of non-thermal plasma combined with catalysts and their application in environmental technology, Catal. Today 211 (2013) 2–8.
[16] K. Hensel, Microdischarges in ceramic foams and honeycombs, Eur. Phys. J. D 54 (2009) 141–148.
[17] A. Rousseau, O. Guaitella, J. Röpcke, L.V. Gatilova, Y.A. Tolmachev, Combination of a pulsed microwave plasma with a catalyst for acetylene oxidation, Appl. Phys. Lett. 85 (2004) 2199–2201.
[18] H.H. Kim, A. Ogata, Y.-H. Song, Propagation of surface streamers on the surface of HSY zeolites-supported silver nanoparticles, IEEE Trans. Plasma Sci. 39 (2011) 2220–2221.
[19] H.H. Kim, A. Ogata, Interaction of nonthermal plasma with catalyst for the air

pollution control, Int. J. Plasma Environ. Sci. Technol. 6 (2012) 43–48.
[20] H.H. Kim, Y. Teramoto, T. Sano, N. Negishi, A. Ogata, Effects of Si/Al ratio on the interaction of nonthermal plasma and Ag/HY catalysts, Appl. Catal. B: Environ. 166–167 (2015) 9–17.
[21] X. Tu, H.J. Gallon, J.C. Whitehead, Transition behavior of packed-bed dielectric barrier discharge in argon, IEEE Trans. Plasma Sci. 39 (2011) 2172–2173.
[22] J.S. Chang, K.G. Kostov, K. Urashima, T. Yamamoto, Y. Okayasu, T. Kato, T. Iwaizumi, K. Yoshimura, Removal of NF_3 from semiconductor-process flue gases by tandem packed-bed plasma and adsorbent hybrid systems, IEEE Trans. Ind. Appl. 36 (2000) 1251–1259.
[23] K. Takaki, J.-S. Chang, K.G. Kostov, Atmospheric pressure of nitrogen plasmas in a ferroelectric packed bed barrier discharge reactor. Part I. Modeling, IEEE Trans. Dielectr. Electr. Insul. 11 (2004) 481–490.
[24] W.S. Kang, J.M. Park, Y. Kim, S.H. Hong, Numerical study on influences of barrier arrangements on dielectric barrier discharge characteristics, IEEE Trans. Plasma Sci. 31 (2003) 504–510.
[25] H. Russ, M. Neiger, J.E. Lang, Simulation of micro discharges for the optimization of energy requirements for removal of NO_x from exhaust gases, IEEE Trans. Plasma Sci. 27 (1999) 38–39.
[26] N.Y. Babaeva, A.N. Bhoj, M.J. Kushner, Streamer dynamics in gases containing dust particles, Plasma Sources Sci. Technol. 15 (2006) 591–602.
[27] J. Kruszelnicki, K.W. Engeling, J.E. Foster, Z. Xiong, M.J. Kushner, Propagation of negative electric discharges through 2-dimensional packed bed reactors, J. Phys. D: Appl. Phys. 50 (2017) 025203.
[28] W.S. Kang, H.H. Kim, Y. Teramoto, A. Ogata, J.Y. Lee, D.W. Kim, M. Hur, Y.H. Song, Surface streamer propagations on an alumina bead: experimental observation and numerical modelling, Plasma Sources Sci. Technol. 27 (2018) 015018.
[29] K. Van Laer, A. Bogaerts, Fluid modelling of a packed bed dielectric barrier discharge plasma reactor, Plasma Sources Sci. Technol. 25 (2016) 015002.
[30] K. Van Laer, A. Bogaerts, Influence of gap size and dielectric constant of the packing material on the plasma behaviour in a packed bed DBD reactor: a fluid modelling study, Plasma Process. Polym. 14 (2017) e1600129.
[31] K. Van Laer, A. Bogaerts, How bead size and dielectric constant affect the plasma behaviour in a packed bed plasma reactor: a modelling study, Plasma Sources Sci. Technol. 26 (2017) 085007.
[32] W. Wang, H.H. Kim, K. Van Laer, A. Bogaerts, Streamer propagation in a packed bed plasma reactor for plasma catalysis applications, Chem. Eng. J. 334 (2018) 2467–2479.
[33] Y. Zhang, H.-Y. Wang, W. Jiang, A. Bogaerts, Two-dimensional particle-in cell/Monte Carlo simulations of a packed-bed dielectric barrier discharge in air at atmospheric pressure, New J. Phys. 17 (2015) 083056.
[34] M.-X. Gao, Y. Zhang, H.-Y. Wang, B. Guo, Q.-Z. Zhang, A. Bogaerts, Mode transition of filaments in packed-bed dielectric barrier discharges, Catalysts 8 (2018) 248.
[35] Q.-Z. Zhang, A. Bogaerts, Plasma streamer propagation in structured catalysts, Plasma Sources Sci. Technol. 27 (2018) 105013.
[36] F. Holzer, U. Roland, F.-D. Kopinke, Combination of non-thermal plasma and heterogeneous catalysis for oxidation of volatile organic compounds: part 1. Accessibility of the intra-particle volume, Appl. Catal. B: Environ. 38 (2002) 163–181.
[37] U. Roland, F. Holzer, F.-D. Kopinke, Combination of non-thermal plasma and heterogeneous catalysis for oxidation of volatile organic compounds: part 2. Ozone decomposition and deactivation of γ-Al_2O_3, Appl. Catal. B: Environ. 58 (2005) 217–226.
[38] K. Hensel, S. Katsura, A. Mizuno, DC microdischarges inside porous ceramics, IEEE Trans. Plasma Sci. 33 (2005) 574–575.
[39] K. Hensel, V. Martisovits, Z. Machala, M. Janda, M. Lestinsky, P. Tardiveau, A. Mizuno, Electrical and optical properties of AC microdischarges in porous ceramics, Plasma Process. Polym. 4 (2007) 682–693.
[40] A.N. Bhoj, M.J. Kushner, Multi-scale simulation of functionalization of rough polymer surfaces using atmospheric pressure plasmas, J. Phys. D: Appl. Phys. 39 (2006) 1594–1598.
[41] A.N. Bhoj, M.J. Kushner, Repetitively pulsed atmospheric pressure discharge treatment of rough polymer surfaces: I. Humid air discharges, Plasma Sources Sci. Technol. 17 (2008) 035024.
[42] A.N. Bhoj, M.J. Kushner, Repetitively pulsed atmospheric pressure discharge treatment of rough polymer surfaces: II. Treatment of micro-beads in $He/NH_3/H_2O$ and $He/O_2/H_2O$ mixtures, Plasma Sources Sci. Technol. 17 (2008) 035025.
[43] X.M. Wang, J.E. Foster, M.J. Kushner, Plasma propagation through porous dielectric sheets, IEEE Trans. Plasma Sci. 39 (2011) 2244–2245.
[44] H. Cheng, X. Liu, X. Lu, D. Liu, Active species delivered by dielectric barrier discharge filaments to bacteria biofilms on the surface of apple, Phys. Plasmas 23 (2016) 073517.
[45] Y.-R. Zhang, K. Van Laer, E.C. Neyts, A. Bogaerts, Can plasma be formed in catalyst pores? A modeling investigation, Appl. Catal. B: Environ. 185 (2016) 56–67.
[46] Y.-R. Zhang, E.C. Neyts, A. Bogaerts, Influence of the material dielectric constant on plasma generation inside catalyst pores, J. Phys. Chem. C 120 (2016) 25923–25934.
[47] Y.-R. Zhang, E.C. Neyts, A. Bogaerts, Enhancement of plasma generation in catalyst pores with different shapes, Plasma Sources Sci. Technol. 27 (2018) 055008.
[48] Y. Zhang, H.-Y. Wang, Y.-R. Zhang, A. Bogaerts, Formation of microdischarges inside a mesoporous catalyst in dielectric barrier discharge plasmas, Plasma Sources Sci. Technol. 26 (2017) 054002.
[49] Q.-Z. Zhang, A. Bogaerts, Propagation of a plasma streamer in catalyst pores, Plasma Sources Sci. Technol. 27 (2018) 035009.
[50] Q.-Z. Zhang, W.-Z. Wang, A. Bogaerts, Importance of surface charging during plasma streamer propagation in catalyst pores, Plasma Sources Sci. Technol. 27 (2018) 065009.
[51] H.Y. Wang, W. Jiang, Y.-N. Wang, Implicit and electrostatic particle-in-cell/Monte Carlo model in two-dimensional and axisymmetric geometry: I. Analysis of numerical techniques, Plasma Sources Sci. Technol. 19 (2010) 045023.
[52] W. Jiang, H.Y. Wang, Z.H. Bi, Y.N. Wang, Implicit and electrostatic particle-in-cell/Monte Carlo model in two-dimensional and axisymmetric geometry: II. Self-bias voltage effects in capacitively coupled plasmas, Plasma Sources Sci. Technol. 20 (2010) 035013.
[53] M.B. Zheleznyak, A.K. Mnatsakanyan, S.V. Sizykh, Photoionization of nitrogen and oxygen mixtures by radiation from a gas discharge, Teplofz. Vys. Temp. 20 (1982) 423–428.
[54] J. Teunissen, U. Ebert, PIC-MCC simulations of discharge inception around a sharp anode in nitrogen/oxygen mixtures, Plasma Sources Sci. Technol. 25 (2016) 044005.
[55] I. Michielsen, Y. Uytdenhouwen, J. Pype, B. Michielsen, J. Mertens, F. Reniers, V. Meynen, A. Bogaerts, CO_2 dissociation in a packed bed DBD reactor: first steps towards a better understanding of plasma catalysis, Chem. Eng. J. 326 (2017) 477–488.
[56] Y. Uytdenhouwen, S. Van Alphen, I. Michielsen, V. Meynen, P. Cool, A. Bogaerts, A packed-bed DBD micro plasma reactor for CO2 dissociation: does size matter? Chem. Eng. J. 348 (2018) 557–568.
[57] W.S. Kang, D.H. Lee, J.-O. Lee, M. Hur, Y.-H. Song, Combination of plasma with a honeycomb-structured catalyst for automobile exhaust treatment, Environ. Sci. Technol. 47 (2013) 11358–11362.
[58] H.H. Kim, Y. Teramoto, N. Negishi, A. Ogata, A multidisciplinary approach to understand the interactions of nonthermal plasma and catalyst: a review, Catal. Today 256 (2015) 13–22.
[59] J. Hong, S. Pancheshnyi, E. Tam, J.J. Lowke, S. Prawer, A.B. Murphy, Kinetic modelling of NH_3 production in N_2-H_2 non-equilibrium atmospheric-pressure plasma catalysis, J. Phys. D: Appl. Phys. 50 (2017) 154005.
[60] J. Shah, W. Wang, A. Bogaerts, M.L. Carreon, Ammonia synthesis by radio frequency plasma catalysis: revealing the underlying mechanisms, ACS Appl. Energy Mater. 1 (2018) 4824–4839.